Secondary Processes Dominate the Quiescent, Spontaneous Aggregation of α-Synuclein at Physiological pH with Sodium Salts

Robert I. Horne[1*], Michael A. Metrick II[1,2*], Wing Man[1],
Dillon Rinauro[1], Z. Faidon Brotzakis[1], Sean Chia[1,3], Georg Meisl[1]
and Michele Vendruscolo[1+]

[1]Centre for Misfolding Diseases, Yusuf Hamied Department of Chemistry, University of Cambridge, Cambridge CB2 1EW, UK
[2]College of Medicine, University of Illinois at Chicago, Chicago IL 60612, USA
*[3]Bioprocessing Technology Institute, Agency of Science, Technology and Research (A*STAR), 138668, Singapore*

[+]mv245@cam.ac.uk
**Equal contributions*

Keywords
Parkinson's disease; protein misfolding; spontaneous α-synuclein aggregation; kinetic mechanisms

Abstract

The accurate recapitulation in an in vitro assay of the aggregation process of α-synuclein in Parkinson's disease has been a significant challenge. As α-synuclein does not aggregate spontaneously in most currently used in vitro assays, to achieve aggregation on accessible timescales, primary nucleation is triggered by the presence of surfaces such as lipid membranes or interfaces created by shaking. In addition, secondary nucleation is typically only observed by lowering the pH below 5.8. Here we investigated assay conditions to observe spontaneous primary nucleation and secondary nucleation at pH 7.4. Using 400 mM sodium phosphate, we observed quiescent spontaneous aggregation of α-synuclein, and established that this aggregation is dominated by secondary processes. Furthermore, the presence of potassium ions enhanced reproducibility of quiescent α-synuclein aggregation. This work provides a framework for the study of spontaneous α-synuclein aggregation at physiological pH.

Introduction

Alzheimer's disease (AD) and Parkinson's disease (PD) are neurodegenerative conditions increasingly common in our aging societies[1], and still largely incurable. The process of protein misfolding and aggregation, which results in the formation of amyloid deposits, is a hallmark of these diseases and may represent a therapeutic target[2-4]. The recent approval lecanemab[5], an antibody that slows down the cognitive decline in AD by targeting the aggregation of Aβ, which is the main component of amyloid deposits, has strengthened the confidence in the amyloid hypothesis[2, 6]. As a consequence, there has been a renewed interest for therapeutic routes for PD based on the targeting of the aggregation of α-synuclein[7-10], which is a protein found in Lewy bodies[11]. These developments are timely, as no disease-modifying drugs have yet been approved for PD[12].

The rational development of protein aggregation inhibitors can be facilitated by the verification of their mechanism of action through in vitro aggregation assays[13, 14]. Protein aggregation takes place through a complex process that involves a combination of intertwined microscopic steps, including primary nucleation, elongation, and secondary nucleation[15-17]. Therapeutic candidates can exhibit vast differences in potency depending on which microscopic steps they inhibit[14, 18]. This aspect has been illustrated for AD by the clinical trials of aducanumab and gantenerumab, two antibodies targeting Aβ aggregates for removal. The approval of aducanumab and the failure of gantenerumab correlate with the different mechanisms of action of these two antibodies, as aducanumab mainly inhibits secondary nucleation, whereas gantenerumab mainly inhibits elongation[19].

For PD, the aggregation process of α-synuclein (αS) has been investigated through similar methods to those developed for Aβ in AD[20-22]. Observing spontaneous αS aggregation in vitro, however, has been challenging. αS aggregation can be promoted by lipid membranes[20-22] or by shaking, which introduces air-water interfaces[23, 24], and is used in diagnostic assays based on biosamples[25]. The spontaneous aggregation of αS has been recently reported within liquid condensates formed by liquid-liquid phase separation[26]. In these condensates, the concentration of αS reaches millimolar levels, thereby dramatically enhancing the speed of the aggregation process. However, the

quest remains open for assays under conditions where spontaneous αS aggregation can be observed in the absence of condensation.

In this work, we report an assay for the spontaneous, quiescent aggregation of N-terminal acetylated αS at pH 7.4 in the absence of lipid membranes. We build upon previous work towards accessing aggregation at physiological pH, where gentle agitation was used (30 rpm for 2-3 weeks)[27]. Here we enable aggregation over a shorter timescale (1-2 days) under quiescent conditions. We established this assay through an optimisation of assay conditions focusing on the presence of anions and counter cations[28]. Given that poly-anionic co-factors are likely involved in the core fibril structures of αS fibrils of multiple systems atrophy (MSA) and PD[29], we investigated the quiescent aggregation of αS in the presence of sulfate, phosphate, and citrate sodium salts. Such salts induced the quiescent aggregation of αS at physiological pH, where the half time ($t_{1/2}$) of the process, which is indicative of the assay speed, was accelerated and showed good reproducibility. By conducting serial dilutions of initial monomer concentration under different seeding conditions, we found that the kinetics of aggregation followed the behaviour expected for a system dominated by secondary processes, with a weak dependence on monomer concentration.

The assay that we report can serve to supplement existing αS assays, providing a battery of tests to verify the mechanism of action of small molecules that inhibit αS aggregation at physiological pH.

Results and Discussion

Spontaneous, quiescent aggregation of αS in high salt concentrations

Methods in this work were designed to keep ionic strength constant such that the character of ions could be investigated, independent from the effect of the concentration of ions in solution. Assays that use brain-derived seeds designed to achieve faithful strain propagation of MSA and PD aggregates via templating recombinant αS focused on the optimised use of strongly hydrated anions such as sodium citrate[30, 31]. Ensuring retention of the original fibril polymorph during aggregation has proved challenging and requires precise tuning of aggregation

conditions[32]. Thus, we first sought to accelerate the extremely slow kinetics of quiescent aggregation of αS at pH 7.4 which previously required beads and other non-physiological co-factors, in the presence of sodium salts at 1 M ionic strength. The quiescent aggregation of αS was enhanced by the presence of divalent anions including SO_4^{2-} and HPO_4^2 (**Figure S1**). Anions of sodium salts are organised in descending hydration order from left to right. These initial experiments suggested that ionic character, independent of strength and hydration status in the Hofmeister series, is an important factor in quiescent αS aggregation.

We then focused our optimisation efforts on sodium phosphate (NaPi), as its reduction of αS kinetic lag times was most pronounced. It was also suggested from the cryo-EM structures of αS fibrils from MSA, PD, and dementia with Lewy bodies (DLB) patient brain extracts that the inter-filament interface may be packed with di-valent anions such as pyrophosphate[29, 33]. We conducted further optimisation experiments and investigated the role of potassium ions in quiescent αS aggregation, as potassium is the main intracellular cation and could thus be a physiological co-aggregator alongside αS oligomers and fibrils. **Figure S2** shows the effects of increasing NaPi (left to right) in the absence (**Figure S2A**) or presence (**Figure S2B**) of 150 mM KCl on quiescent αS aggregation. A dependence of lag time on NaPi concentration is shown as increasing NaPi accelerates the quiescent reaction. At an identical concentration of NaPi, addition of 150 mM KCl accelerates such lag times as much as 3-fold in the case of 400 mM NaPi. Additionally, deviation from mean aggregation time is lessened in the presence of KCl.

We used circular dichroism (CD) experiments to probe the secondary structure of αS monomers in the various salts in the presence and absence of KCl, finding no significant effects (**Figure S3**). Fibril formation in seeded and unseeded conditions was confirmed via Fourier transform infrared **(**FTIR) spectroscopy and transmission electron microscopy (TEM) (**Figure S4**). We also found that KCl alone was not sufficient to produce mature αS fibrils (**Figure S5**).

With these reaction parameters, an αS aggregation assay could be conducted in two days at pH 7.4. The kinetics of the quiescent aggregation of αS were then investigated via serial dilutions of input monomer under various seeding conditions in order to glean

information on the microscopic mechanisms that drive aggregation[15-17]. We then analyzed the dependence of $t_{1/2}$ against the monomer concentration for an unseeded aggregation allowing derivation of a scaling exponent[17] (**Figure 1A**). This type of analysis was not previously possible for unseeded αS aggregation. The scaling exponent approached the value of -0.5 indicting a weak dependence of the aggregation rate on monomer concentration[17] . The ThT traces used to derive the log plot are displayed in **Figure 1B**. Sigmoidal curves, which are indicative of secondary processes, were observed in quiescent conditions at pH 7.4, in contrast to previous aggregation mechanism investigations of αS which required lowering pH below 6.5 to observe clear signs of secondary processes[20, 34].

We then measured the ThT fluorescence over increasing input αS monomer, each seeded with 2.5 nM preformed αS fibrils produced in identical reaction conditions (**Figure 1C)**. The significant increase in aggregation speed at these low seed concentrations compared to the unseeded reaction further confirms that under these conditions secondary processes dominates the production of new fibrils. The introduction of these small concentrations of seeds significantly reduced the monomer concentration-dependence of the reaction, with $t_{1/2}$ at 2.5 nM seed being effectively independent of the monomer concentration. Elongation became the dominant mechanism when large amounts of preformed fibrils were present. We observed saturation of elongation rates at high seed (5 μM) at different concentrations of αS monomer, analogous to the elongation saturation observed previously[20] at pH 7.4 (**Figure 1D**).

Kinetic analysis of αS aggregation in high salt

A mechanistic analysis of the data is complicated by the slow approach of the kinetic curves to their plateau value, a feature typical of αS aggregation[35]. It likely originates from clumping, sedimentation or other effects not generally modelled explicitly, and leads to a deviation of the fitted curves from the experimental ones close to the plateau. To determine the concentration-dependence of the different aggregation steps, we first fitted the sets of seed concentrations at each monomer concentration, extracting the rates of fibril formation via primary (λ) and secondary (κ) processes at each monomer concentration[13, 16]. These fits are shown in **Figure 2A-D**, while the behaviour of λ and κ with varying monomer concentration is shown in **Figure 2E**. The fits confirm the

strong dominance of secondary processes over primary ones. However, given the low reaction order of the secondary process, it was not possible to determine whether the dominant secondary process was fragmentation or secondary nucleation based on the kinetics alone. This is a well-known effect, as demonstrated previously[35]. We also observed a very strong dependence of primary nucleation on concentration, suggesting a primary reaction order of approximately 13. Given these observations, we then went on to fit all data globally, with a kinetic model that includes a saturated elongation process, a concentration independent secondary process and a primary nucleation process (**Figure S6**). The model matches well the seed dependence, monomer dependence, early time and mid time slopes, but fails to reproduce the slow approach to the plateau, overall supporting the above the mechanistic conclusions. Particularly noticeable is the high reaction order of primary nucleation, suggesting a large nucleus size, in line with the difficulty of triggering primary nucleation in αS aggregation. We furthermore confirm that the behaviour observed here cannot be adequately explained by a model where secondary processes are negligible (**Figure S7**).

Small molecule inhibitors of secondary nucleation in high salt

A set of small molecules previously been identified as αS secondary nucleation inhibitors[36] were also tested here, as a test of both the mechanism of aggregation and the molecules themselves. The two most potent molecules previously reported, I3.02 and I4.05, showed high levels of inhibition (**Figure 3**). The fact that the aggregation reaction in the assay reported in this work can be slowed by inhibitors of secondary nucleation suggests that this process, rather than fragmentation, dominates here. For comparison, Anle-138b, a compound tested for αS aggregation[37], is also shown with no observable inhibition. The plateau drift in the presence of DMSO may have resulted from interactions between the organic solvent and high salt concentration.

Conclusions

In this work we have reported an in vitro aggregation assay to study the spontaneous aggregation of αS under quiescent conditions at physiological pH. This assay adds to an increasing repertoire of seeded and unseeded αS assays (**Table S1**). While

modulating the importance of different microscopic processes by changing solution conditions is well established[20-22, 34], this work provides a framework to observe secondary nucleation processes at neutral pH, and greatly accelerates the primary nucleation of αS without the need of using surfaces or interfaces. We show that both anionic and cationic species were critical to this optimisation, which may function to neutralise side-chain charge along the axis of the growing fibrils. This work is consistent with the finding that structures of αS fibrils from MSA patient brains resolved by cryo-EM revealed unknown electron dense entities packed into the inter-filament interface, surrounded by many positively charged residues, suggesting that charged cofactors may be packed into the inter-filament interfaces. As a mechanistic test, small molecules previously reported to inhibit secondary nucleation also showed significant efficacy, suggesting that secondary nucleation contributes significantly to the aggregation process under the conditions used here. Although it remains to be seen if the in vitro αS assay reported in this work can faithfully replicate ex vivo fibrils, we suggest that this work can inform drug discovery and mechanistic investigations for PD and related synucleinopathies[10, 36, 38].

Materials and Methods

Purification of αS

N-terminal acetylated wild-type αS was purified as described previously[20-22, 34, 39]. Briefly, αS was produced by co-transforming *E. coli* with the pT7–7 plasmid and an expression pACYCduet plasmid encoding a yeast N-terminal acetyltransferase (NatB), provided by Dr. Dan Mulvihill, University of Kent, Canterbury, UK. (24) Recombinant αS was purified as described previously. The plasmid pT7-7 encoding for human αS was transformed into BL21-competent cells alongside an expression pACYCduet plasmid encoding a yeast N-terminal acetyltransferase (NatB), provided by Dr.Dan Mulvihill, University of Kent, Canterbury, UK. Following transformation, competent cells were grown in LB in the presence of ampicillin (100 µg/mL). Cells were induced with IPTG and grown overnight at 37 ^{o}C and harvested by centrifugation in a Beckman Avanti J25 centrifuge with a JA-20 rotor at 5000 rpm (Beckman Coulter, Fullerton, CA). The cell pellet was resuspended in 10 mM Tris, pH 8.0, 1 mM EDTA, 1 mM PMSF and lysed by multiple freeze–thaw cycles and sonication. The cell suspension was boiled

for 20 min and centrifuged at 13,500 rpm with a JA-20 rotor (Beckman Coulter). Streptomycin sulfate was added to the supernatant to a final concentration of 10 mg/mL and the mixture was stirred for 15 min at 4 ºC. After centrifugation at 13,500 rpm, the supernatant was taken with an addition of 0.36 g/mL ammonium sulfate. The solution was stirred for 30 min at 4 ºC and centrifuged again at 13,500 rpm. The pellet was resuspended in 25 mM Tris, pH 7.7, and ion-exchange chromatography was performed using a HQ/M-column of buffer A (25 mM Tris, pH 7.7) and buffer B (25 mM Tris, pH 7.7, 600 mM NaCl). The fractions containing αS (≈ 300 μM) were dialysed overnight against the appropriate buffer. Aliquots were flash-frozen in liquid N2 and stored at −80 °C. The presence of N-terminal acetylation was verified by mass spectrometry and the protein concentration was determined spectrophotometrically using ε275 = 5600 M^{-1} cm^{-1}.

Aggregation assays

All aggregation assays were performed on fresh αS following size exclusion chromatography (SEC) through a Superdex 75 Increase 10/300 GL. Additional uses of excess αS from previous experiments followed a freeze-thaw cycle at -20 ºC, concentration, and further SEC immediately prior to kinetic analysis to remove preformed seeds. αS was exchanged by SEC into 20 mM NaPi pH 7.4 after which it was combined with the designated salts for kinetic analysis. All reactions were performed at 100 uL in Corning 3881 96-well half-area plates at 37 ºC with an aluminium plate sticker to mitigate evaporation. Plates were incubated in FluoStar LITE plate readers (OMEGA) for up to 7 days with periodic ThT fluorescence measurements, in the absence of shaking. Fitting of kinetic models followed the Amylofit recommendations[17]. Elongation experiments were conducted by adding 15 uM preformed fibrils to a dilution series of αS in 400 mM sodium phosphate, 150 mM KCl, pH 7.4 as above. For inhibition testing the molecules (or DMSO alone) were then added at the desired concentration to a final DMSO concentration of 1% (v/v).

Fourier transform infrared (FTIR) spectroscopy

αS fibrils were recovered from completed spontaneous and seeded aggregation assays following plateau of ThT fluorescence. Fibrils were centrifuged at 21300 rcf for 10 min before resuspension in water. Samples were dehydrated under light flow of dry air. FTIR spectra were recorded on a Bruker Vertex 70 FTIR (Billerica, USA) on the

diamond ATR, with 4 cm resolution and a data range of 800–4000 cm^{-1}; the data in the amide peak 1 (1580–1720 cm^{-1}) were analysed. A rubber band baseline correction was applied to the data, before fitting to a Gaussian equation with 4–7 peaks. The area under each peak was integrated to obtain relative compositions of the secondary structure using the following classifications: peaks under 1640 cm^{-1} were assigned to β-sheet structures; peaks from 1640 to 1660 cm^{-1} were assigned to disordered random coils/α-helices, and peaks above 1660 and 1685 cm^{-1} were also assigned to β-sheet structures.

Transmission electron microscopy (TEM)

αS reaction samples were recovered by pipetting up and down after ThT plateau as described above. TEM images were obtained with the assistance of the electron microscopy specialist Dr Heather Greer of the in-house (Department of Chemistry) TEM facility. Copper Quantifoil R2/2 grids (Quantifoil GmbH, Germany) were first glow-discharged before applying 2.5 µL of the samples for 40 seconds. The excess sample was carefully absorbed using blotting paper and then the grids were stained using 1.5 wt% uranyl acetate for 40 seconds. The excess uranyl acetate was removed using blotting paper. Micrographs were acquired using a Talos F200X G2 electron microscope operating at 200 kV (FEI, Hillsboro, Oregon, United States). Digital micrographs were acquired on a Ceta 16M camera with speed enhancement using the EMMENU 4 software package (TVIPS, Munich, Germany). The images were analysed using ImageJ.

Acknowledgements

Michael A. Metrick II would like to acknowledge NIH/Cambridge scholars programme and the Cambridge Trust for financial support. We would also like to thank ARCHER, MARCOPOLO and CIRCE high performance computing resources for the computer time. Z. Faidon Brotzakis would like to acknowledge the Federation of European Biochemical Societies (FEBS) for financial support (LTF). The authors are furthermore grateful for financial support from the Cambridge Centre for Misfolding Diseases. Parts of the figures were created with BioRender.com.

Associated Content

Supporting Information available. This includes initial aggregation experiments with different salts, a summary of previous aggregation conditions for αS, CD experiments investigating salt effects on folding, structural characterization of the αS fibrils via FTIR and TEM and a global fit of all experiments presented in **Figures 1** and **2**. This information is available free of charge via the Internet at http://pubs.acs.org.

Author Contributions

RIH, MAM, WM and MV designed research; all authors performed research, analyzed data and wrote the manuscript.

Conflicts of Interest

RIH is a consultant of WaveBreak Therapeutics (formerly Wren Therapeutics). MAM has been a consultant of WaveBreak Therapeutics. SC has been an employee of WaveBreak Therapeutics. GM is an employee of WaveBreak Therapeutics. MV is a founder of WaveBreak Therapeutics.

References

(1) Nichols, E.; Steinmetz, J. D.; Vollset, S. E.; Fukutaki, K.; Chalek, J.; Abd-Allah, F.; Abdoli, A.; Abualhasan, A.; Abu-Gharbieh, E.; Akram, T. T. Estimation of the global prevalence of dementia in 2019 and forecasted prevalence in 2050: an analysis for the Global Burden of Disease Study 2019. *Lancet Public Health* **2022**, *7* (2), e105-e125.

(2) Hampel, H.; Hardy, J.; Blennow, K.; Chen, C.; Perry, G.; Kim, S. H.; Villemagne, V. L.; Aisen, P.; Vendruscolo, M.; Iwatsubo, T. The amyloid-β pathway in Alzheimer's disease. *Mol. Psychiatry* **2021**, *26* (10), 5481-5503.

(3) Knowles, T. P.; Vendruscolo, M.; Dobson, C. M. The amyloid state and its association with protein misfolding diseases. *Nature reviews Molecular cell biology* **2014**, *15* (6), 384-396.

(4) Eisenberg, D.; Jucker, M. The amyloid state of proteins in human diseases. *Cell* **2012**, *148* (6), 1188-1203.

(5) Van Dyck, C. H.; Swanson, C. J.; Aisen, P.; Bateman, R. J.; Chen, C.; Gee, M.; Kanekiyo, M.; Li, D.; Reyderman, L.; Cohen, S. Lecanemab in early Alzheimer's disease. *N. Engl. J. Med.* **2023**, *388* (1), 9-21.
(6) Hardy, J. A.; Higgins, G. A. Alzheimer's disease: the amyloid cascade hypothesis. *Science* **1992**, *256* (5054), 184-185.
(7) Murray, K. A.; Hu, C. J.; Pan, H.; Lu, J.; Abskharon, R.; Bowler, J. T.; Rosenberg, G. M.; Williams, C. K.; Elezi, G.; Balbirnie, M. Small molecules disaggregate alpha-synuclein and prevent seeding from patient brain-derived fibrils. *Proc. Natl. Acad. Sci. USA* **2023**, *120* (7), e2217835120.
(8) Wu, S.; Hernandez Villegas, N. C.; Schekman, R. Chemical disaggregation of alpha-synuclein fibrils as a therapy for synucleinopathies. *Proc. Natl. Acad. Sci. USA* **2023**, *120* (11), e2300965120.
(9) Price, D. L.; Koike, M. A.; Khan, A.; Wrasidlo, W.; Rockenstein, E.; Masliah, E.; Bonhaus, D. The small molecule alpha-synuclein misfolding inhibitor, NPT200-11, produces multiple benefits in an animal model of Parkinson's disease. *Sci. Rep.* **2018**, *8* (1), 16165.
(10) Chia, S.; Faidon Brotzakis, Z.; Horne, R. I.; Possenti, A.; Mannini, B.; Cataldi, R.; Nowinska, M.; Staats, R.; Linse, S.; Knowles, T. P. Structure-Based Discovery of Small-Molecule Inhibitors of the Autocatalytic Proliferation of α-Synuclein Aggregates. *Mol. Pharm.* **2022**.
(11) Spillantini, M. G.; Schmidt, M. L.; Lee, V. M.-Y.; Trojanowski, J. Q.; Jakes, R.; Goedert, M. α-Synuclein in Lewy bodies. *Nature* **1997**, *388* (6645), 839-840.
(12) McFarthing, K.; Rafaloff, G.; Baptista, M.; Mursaleen, L.; Fuest, R.; Wyse, R. K.; Stott, S. R. Parkinson's disease drug therapies in the clinical trial pipeline: 2022 update. *Journal of Parkinson's Disease* **2022**, (Preprint), 1-10.
(13) Michaels, T. C.; Šarić, A.; Meisl, G.; Heller, G. T.; Curk, S.; Arosio, P.; Linse, S.; Dobson, C. M.; Vendruscolo, M.; Knowles, T. P. Thermodynamic and kinetic design principles for amyloid-aggregation inhibitors. *Proc. Natl. Acad. Sci. USA* **2020**, *117* (39), 24251-24257.
(14) Chia, S.; Habchi, J.; Michaels, T. C.; Cohen, S. I.; Linse, S.; Dobson, C. M.; Knowles, T. P.; Vendruscolo, M. SAR by kinetics for drug discovery in protein misfolding diseases. *Proceedings of the National Academy of Sciences* **2018**, *115* (41), 10245-10250.

(15) Knowles, T. P.; Waudby, C. A.; Devlin, G. L.; Cohen, S. I.; Aguzzi, A.; Vendruscolo, M.; Terentjev, E. M.; Welland, M. E.; Dobson, C. M. An analytical solution to the kinetics of breakable filament assembly. *Science* **2009**, *326* (5959), 1533-1537.
(16) Cohen, S. I.; Vendruscolo, M.; Dobson, C. M.; Knowles, T. P. From macroscopic measurements to microscopic mechanisms of protein aggregation. *J. Mol. Biol.* **2012**, *421* (2-3), 160-171.
(17) Meisl, G.; Kirkegaard, J. B.; Arosio, P.; Michaels, T. C.; Vendruscolo, M.; Dobson, C. M.; Linse, S.; Knowles, T. P. Molecular mechanisms of protein aggregation from global fitting of kinetic models. *Nature protocols* **2016**, *11* (2), 252-272.
(18) Michaels, T. C.; Dear, A. J.; Cohen, S. I.; Vendruscolo, M.; Knowles, T. P. Kinetic profiling of therapeutic strategies for inhibiting the formation of amyloid oligomers. *The Journal of Chemical Physics* **2022**, *156* (16), 164904.
(19) Linse, S.; Scheidt, T.; Bernfur, K.; Vendruscolo, M.; Dobson, C. M.; Cohen, S. I.; Sileikis, E.; Lundqvist, M.; Qian, F.; O'Malley, T. Kinetic fingerprints differentiate the mechanisms of action of anti-Aβ antibodies. *Nat. Struct. Mol. Biol.* **2020**, *27* (12), 1125-1133.
(20) Buell, A. K.; Galvagnion, C.; Gaspar, R.; Sparr, E.; Vendruscolo, M.; Knowles, T. P.; Linse, S.; Dobson, C. M. Solution conditions determine the relative importance of nucleation and growth processes in α-synuclein aggregation. *Proc. Natl. Acad. Sci. USA* **2014**, *111* (21), 7671-7676.
(21) Galvagnion, C.; Buell, A. K.; Meisl, G.; Michaels, T. C.; Vendruscolo, M.; Knowles, T. P.; Dobson, C. M. Lipid vesicles trigger α-synuclein aggregation by stimulating primary nucleation. *Nature chemical biology* **2015**, *11* (3), 229-234.
(22) Galvagnion, C.; Brown, J. W.; Ouberai, M. M.; Flagmeier, P.; Vendruscolo, M.; Buell, A. K.; Sparr, E.; Dobson, C. M. Chemical properties of lipids strongly affect the kinetics of the membrane-induced aggregation of α-synuclein. *Proc. Natl. Acad. Sci. USA* **2016**, *113* (26), 7065-7070.
(23) Cremades, N.; Cohen, S. I.; Deas, E.; Abramov, A. Y.; Chen, A. Y.; Orte, A.; Sandal, M.; Clarke, R. W.; Dunne, P.; Aprile, F. A. Direct observation of the interconversion of normal and toxic forms of α-synuclein. *Cell* **2012**, *149* (5), 1048-1059.
(24) Zhou, J.; Ruggeri, F. S.; Zimmermann, M. R.; Meisl, G.; Longo, G.; Sekatskii, S. K.; Knowles, T. P.; Dietler, G. Effects of sedimentation, microgravity, hydrodynamic

mixing and air–water interface on α-synuclein amyloid formation. *Chem. Sci.* **2020**, *11* (14), 3687-3693.
(25) Siderowf, A.; Concha-Marambio, L.; Lafontant, D.-E.; Farris, C. M.; Ma, Y.; Urenia, P. A.; Nguyen, H.; Alcalay, R. N.; Chahine, L. M.; Foroud, T. Assessment of heterogeneity among participants in the Parkinson's Progression Markers Initiative cohort using α-synuclein seed amplification: a cross-sectional study. *Lancet Neurol.* **2023**, *22* (5), 407-417.
(26) Dada, S. T.; Hardenberg, M. C.; Toprakcioglu, Z.; Mrugalla, L. K.; Cali, M. P.; McKeon, M. O.; Klimont, E.; Michaels, T. C.; Knowles, T. P.; Vendruscolo, M. Spontaneous nucleation and fast aggregate-dependent proliferation of α-synuclein aggregates within liquid condensates at neutral pH. *Proceedings of the National Academy of Sciences* **2023**, *120* (9), e2208792120.
(27) Kumari, P.; Ghosh, D.; Vanas, A.; Fleischmann, Y.; Wiegand, T.; Jeschke, G.; Riek, R.; Eichmann, C. Structural insights into α-synuclein monomer–fibril interactions. *Proceedings of the National Academy of Sciences* **2021**, *118* (10), e2012171118.
(28) Meisl, G.; Yang, X.; Dobson, C. M.; Linse, S.; Knowles, T. P. Modulation of electrostatic interactions to reveal a reaction network unifying the aggregation behaviour of the Aβ42 peptide and its variants. *Chem Sci* **2017**, *8* (6), 4352-4362.
(29) Yang, Y.; Shi, Y.; Schweighauser, M.; Zhang, X.; Kotecha, A.; Murzin, A. G.; Garringer, H. J.; Cullinane, P. W.; Saito, Y.; Foroud, T. Structures of α-synuclein filaments from human brains with Lewy pathology. *Nature* **2022**, *610* (7933), 791-795.
(30) Martinez-Valbuena, I.; Visanji, N. P.; Kim, A.; Lau, H. H.; So, R. W.; Alshimemeri, S.; Gao, A.; Seidman, M. A.; Luquin, M. R.; Watts, J. C. Alpha-synuclein seeding shows a wide heterogeneity in multiple system atrophy. *Transl. Neurodegener.* **2022**, *11* (1), 7.
(31) Metrick, M. A.; do Carmo Ferreira, N.; Saijo, E.; Hughson, A. G.; Kraus, A.; Orrú, C.; Miller, M. W.; Zanusso, G.; Ghetti, B.; Vendruscolo, M. Million-fold sensitivity enhancement in proteopathic seed amplification assays for biospecimens by Hofmeister ion comparisons. *Proceedings of the National Academy of Sciences* **2019**, *116* (46), 23029-23039.
(32) Lövestam, S.; Schweighauser, M.; Matsubara, T.; Murayama, S.; Tomita, T.; Ando, T.; Hasegawa, K.; Yoshida, M.; Tarutani, A.; Hasegawa, M. Seeded assembly in vitro does not replicate the structures of α ‐ synuclein filaments from multiple system atrophy. *FEBS open bio* **2021**, *11* (4), 999-1013.

(33) Schweighauser, M.; Shi, Y.; Tarutani, A.; Kametani, F.; Murzin, A. G.; Ghetti, B.; Matsubara, T.; Tomita, T.; Ando, T.; Hasegawa, K. Structures of α-synuclein filaments from multiple system atrophy. *Nature* **2020**, *585* (7825), 464-469.
(34) Flagmeier, P.; Meisl, G.; Vendruscolo, M.; Knowles, T. P.; Dobson, C. M.; Buell, A. K.; Galvagnion, C. Mutations associated with familial Parkinson's disease alter the initiation and amplification steps of α-synuclein aggregation. *Proc. Natl. Acad. Sci. USA* **2016**, *113* (37), 10328-10333.
(35) Gaspar, R.; Meisl, G.; Buell, A. K.; Young, L.; Kaminski, C. F.; Knowles, T. P.; Sparr, E.; Linse, S. Secondary nucleation of monomers on fibril surface dominates α-synuclein aggregation and provides autocatalytic amyloid amplification. *Q. Rev. Bioph.* **2017**, *50*, e6.
(36) Horne, R. I.; Possenti, A.; Chia, S.; Brotzakis, F.; Staats, R.; Habchi, J.; Vendruscolo, M. A Machine Learning Approach to Identify Specific Small Molecule Inhibitors of Secondary Nucleation in α-Synuclein Aggregation. *bioRxiv* **2021**, 2021.2011. 2010.468009.
(37) Wagner, J.; Ryazanov, S.; Leonov, A.; Levin, J.; Shi, S.; Schmidt, F.; Prix, C.; Pan-Montojo, F.; Bertsch, U.; Mitteregger-Kretzschmar, G. Anle138b: a novel oligomer modulator for disease-modifying therapy of neurodegenerative diseases such as prion and Parkinson's disease. *Acta Neuropathol.* **2013**, *125*, 795-813.
(38) Horne, R. I.; Murtada, M. H.; Huo, D.; Brotzakis, Z. F.; Gregory, R. C.; Possenti, A.; Chia, S.; Vendruscolo, M. Exploration and Exploitation Approaches Based on Generative Machine Learning to Identify Potent Small Molecule Inhibitors of α-Synuclein Secondary Nucleation. *J. Chem. Theory Comput.* **2023**.
(39) Bell, R.; Castellana-Cruz, M.; Nene, A.; Thrush, R. J.; Xu, C. K.; Kumita, J. R.; Vendruscolo, M. Effects of N-terminal acetylation on the aggregation of disease-related α-synuclein variants. *J. Mol. Biol.* **2023**, *435* (1), 167825.

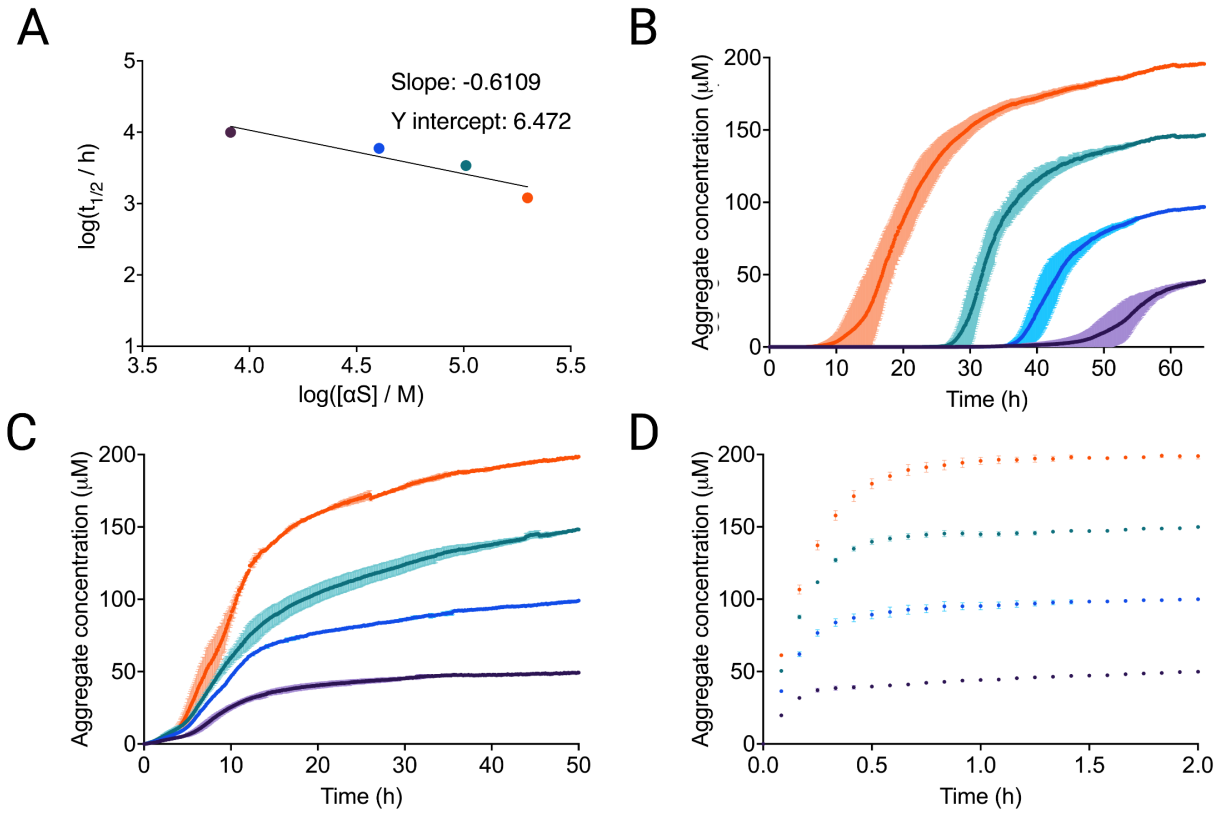

Figure 1. **Spontaneous, quiescent aggregation of αS in 150 mM KCl and 400 mM NaPi.** αS monomer concentrations are: 50 μM (purple), 100 μM (blue), 150 μM (teal), 200 μM (orange). (**A**) The scaling exponent, which is the slope of the log-log plot of the monomer concentration (m_0) vs half time ($t_{1/2}$) for the unseeded aggregation under this condition, is close to -0.5, indicating secondary processes independent from monomer concentration[35]. (**B**) Aggregation kinetics of unseeded αS. (**C**) Aggregation kinetics of αS in the presence of low seed concentration (2.5 nM). (**D**) Aggregation kinetics of αS in the presence of high seed concentration (5 μM). The endpoints are normalised to the αS monomer concentration at the end of the experiment, which was detected via the Pierce™ BCA Protein Assay.

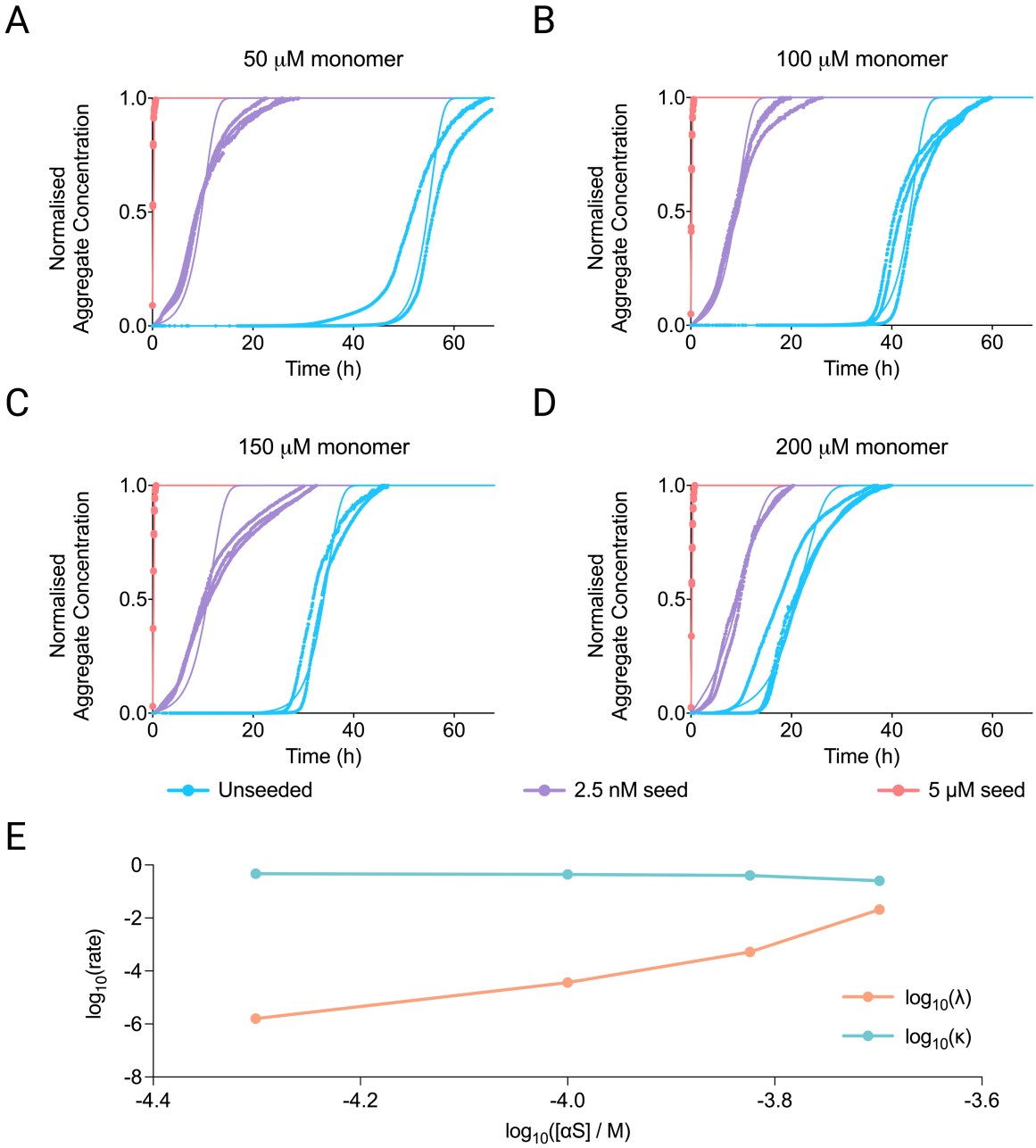

Figure 2. Kinetic analysis of αS aggregation in 150 mM KCl and 400 mM NaPi. (A-D) Fitting of aggregation kinetics with data (points) and fits (solid lines) shown side by side against time (h). Monomer concentrations are: 50 μM (**A**), 100 μM (**B**), 150 μM (**C**), 200 μM (**D**). (**E**) Rates of primary (λ) and secondary (κ) processes as a function of monomer concentration on a double logarithmic plot. Secondary processes are essentially independent of monomer concentration, whereas primary processes are strongly dependent on monomer concentration. There is also a curvature in the double logarithmic plot of primary nucleation rate versus concentration, implying a change of the rate-determining step[17].

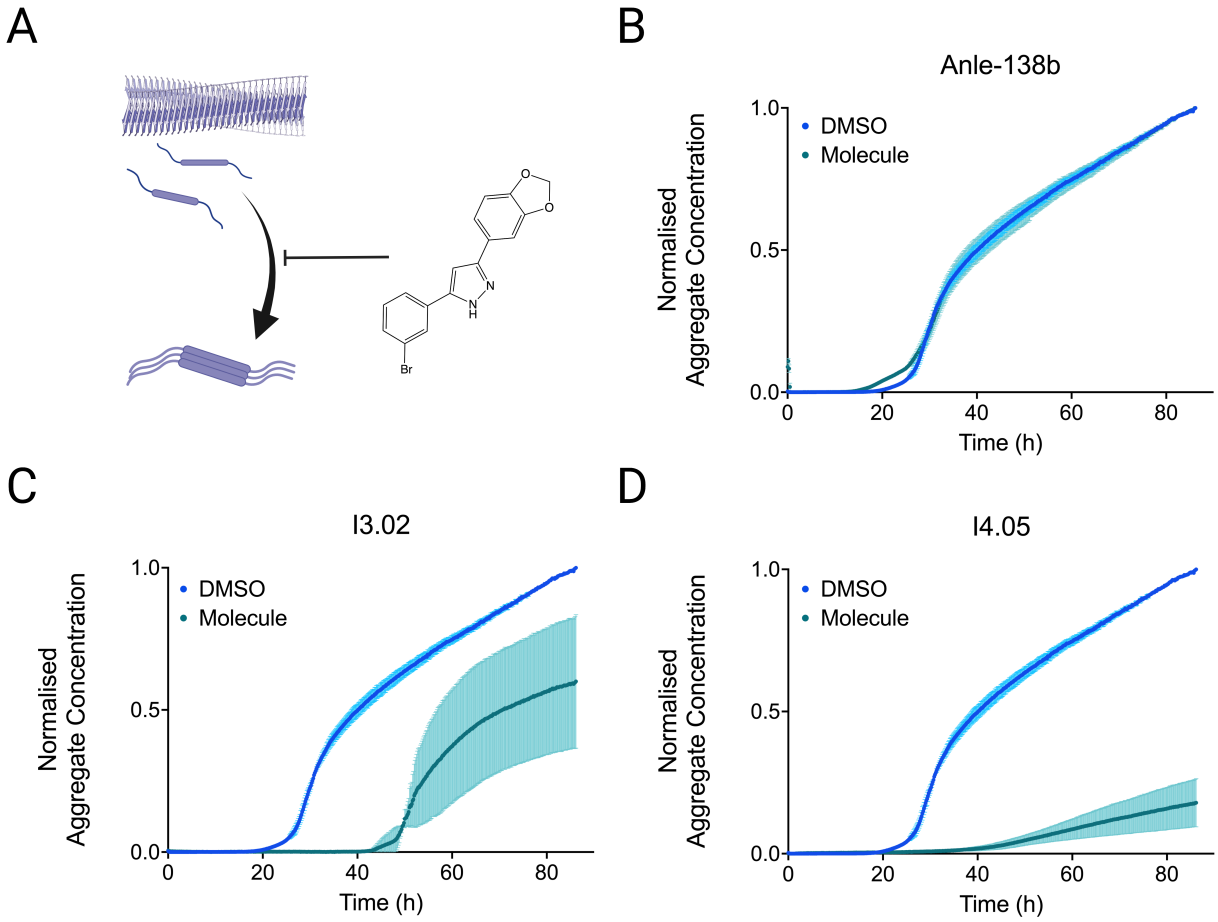

Figure 3. Small molecule inhibitors of secondary nucleation in the aggregation assay reported in this work. (**A**) Schematic of the aggregation process. A dominant mechanism in oligomer formation is the nucleation of aggregates from the surfaces of existing ones (secondary nucleation). Small molecules can block this process by blocking the nucleation sites on the surface of the fibrils[10, 36, 38]. (**B-D**) Kinetic traces are shown of a 100 μM solution of αS pH 7.4, 37°C with 150 mM KCl and 400 mM NaPi in the presence of 1% DMSO (light blue) or at 50 μM molecule (teal): Anle-138b (**B**), I3.02 (**C**), and I4.05 (**C**).

Table of Contents (TOC) Graphic